Desert dust suppressing precipitation: A possible desertification feedback loop

Daniel Rosenfeld*, Yinon Rudich†‡, and Ronen Lahav*

*Institute of Earth Sciences, The Hebrew University, Jerusalem 91904, Israel; and †Department of Environmental Sciences, Weizmann Institute, Rehovot 76100, Israel

Communicated by A. R. Ravishankara, National Oceanic and Atmospheric Administration, Boulder, CO, March 13, 2001 (received for review October 11, 2000)

The effect of desert dust on cloud properties and precipitation has so far been studied solely by using theoretical models, which predict that rainfall would be enhanced. Here we present observations showing the contrary; the effect of dust on cloud properties is to inhibit precipitation. Using satellite and aircraft observations we show that clouds forming within desert dust contain small droplets and produce little precipitation by drop coalescence. Measurement of the size distribution and the chemical analysis of individual Saharan dust particles collected in such a dust storm suggest a possible mechanism for the diminished rainfall. The detrimental impact of dust on rainfall is smaller than that caused by smoke from biomass burning or anthropogenic air pollution, but the large abundance of desert dust in the atmosphere renders it important. The reduction of precipitation from clouds affected by desert dust can cause drier soil, which in turn raises more dust, thus providing a possible feedback loop to further decrease precipitation. Furthermore, anthropogenic changes of land use exposing the topsoil can initiate such a desertification feedback process.

Satellite Observations of Cloud-Dust Interactions

The three major sources of aerosols in the atmosphere are desert dust, smoke from biomass burning, and anthropogenic air pollution. The latter two are recognized as sources of large concentrations of small cloud condensation nuclei (CCN), which lead to the formation of a high concentration of small cloud droplets and therefore to an increased cloud albedo (1) and suppressed precipitation (2). Desert dust that passes over polluted areas often can be coated by sulfur due to chemical processes on their surface (3). These particles then can serve as giant CCN, which may enhance the collision and coalescence of droplets and therefore increase warm precipitation formation and decrease the clouds' albedo (4). However, our satellite, aircraft, and laboratory observations show that mineral dust suppresses precipitation. Possible causes for this apparent contradiction are discussed later.

Data from the Advanced Very High-Resolution Radiometer (AVHRR) onboard the National Oceanographic and Atmospheric Administration satellite were used for retrieving properties of clouds that formed during a heavy dust storm in March 1998 over the Eastern Mediterranean. The satellite image is shown in Fig. 1, using the microphysical color scheme of Rosenfeld and Lensky (5). The dust rapidly advected from the Sahara through Southern Israel, Jordan, and Syria and curled back through Turkey into the center of a cyclonic depression over Cyprus. A "tongue" of dust-free air converged into the cyclone from the north and west. Shallow convective clouds of similar depth and shapes developed over the sea and the adjacent land in both dust laden and dust-free regions. Retrieval of cloud microstructure (see Fig. 2) reveals that the droplets in clouds that formed in the dust-free zone had large effective radii (r_e) that steeply increased with height or with decreasing cloud top temperature (T). These observations indicate ample coalescence and possible precipitation. In contrast, clouds of comparable depth that formed in the dusty air had much smaller particles, with $r_e < 14$ μm, the minimal size required for the onset of precipitation (6). These clouds had little coalescence and formed no precipitation (5). Cloud particles in the dusty air exceeded the 14-μm precipitation threshold only when the clouds grew vertically to heights greater than the -12°C isotherm level (see T-r_e relation of frame 6 in Fig. 2). It is not known whether the larger r_e at $T < -12$°C was caused by coalescence or the formation of the ice phase. The clouds did not show any obvious change of shape, organization, or cloud base temperature. We therefore conclude that the microphysical changes are the result of the desert dust present in the clouds.

A point of concern for the validity of the satellite retrievals is the possibility that desert dust above and in the clouds would distort the measurement of the cloud droplets effective radius (r_e). A quantitative inspection using the visible and thermal channels of areas 4–6 in Fig. 1 shows that clouds cast shadows on the dust layer only when their tops exceed the +3°C isotherm, which is taller than 1,500 m above sea level. This means that only the cloud bases are immersed in the dust layer. Further north, near area 1, the cloud tops had to exceed the -3°C isotherm before breaking through the dust layer and casting shadows on it. This finding indicates that there is no interference of intervening dust between the middle and upper portions of the clouds analyzed in Fig. 2 and the satellite. The dust particles that are interstitial or reside inside the cloud droplets as CCN can still potentially affect the inferred droplet radius. From the calculations of Levi (7), assuming the refraction index of dust at 3.7 μm to be 1.27 + i0.01075 (the absorption is three times larger for dust than for water), the single scattering albedo of droplets with embedded desert dust is reduced when the radius of the immersed dust particle approaches the radius of the cloud drop. Wet dust particles thus would reduce and not increase the cloud reflectance at 3.7 μm, possibly causing an overestimate of the effective radius. The optical properties of the droplets do not change when the water droplet is larger than the embedded dust particle (7); therefore, the way dust affects the 3.7-μm reflectance eliminates the concern that the inferred reduction of the effective radius in clouds is caused by the optical properties of the dust, thus confirming the observation that the size of the droplets in dust-laden clouds is truly smaller than that in dust-free clouds.

In addition, the concern that the enhanced reflectance of the clouds at 3.7 μm may be caused by the direct contribution of the dust itself can be alleviated by the following measurement: A semi-isolated cloud in the dusty area over the Mediterranean sea east of Cyprus had a 3.7-μm reflectance of 25% and calculated r_e of 6 μm. The reflectance of an adjacent dusty cloudless air over sea was 14%, and the sea surface reflectance in the dust-free air

Abbreviations: CCN, cloud condensation nuclei; TRMM, Tropical Rainfall Measuring Mission; GMT, Greenwich mean time; SEM, scanning electron microscope; AERONET, Aerosol Robotic Network.

‡To whom reprint requests should be addressed.

The publication costs of this article were defrayed in part by page charge payment. This article must therefore be hereby marked "*advertisement*" in accordance with 18 U.S.C. §1734 solely to indicate this fact.

GEOPHYSICS

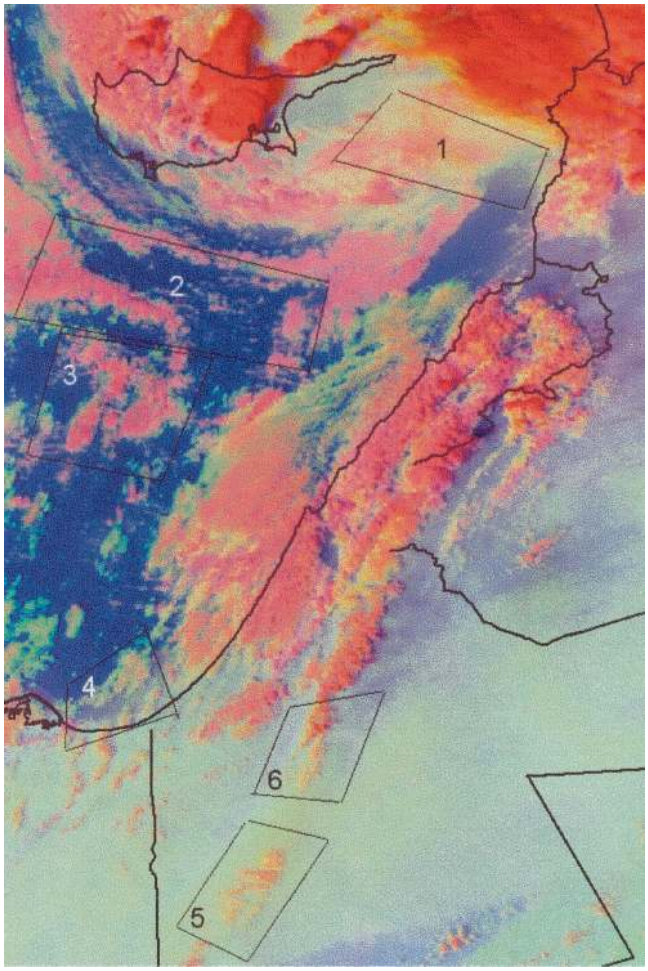

Fig. 1. Impact of dust storm on cloud microstructure over the eastern Mediterranean. The image was obtained by a National Oceanographic and Atmospheric Administration advanced very high-resolution radiometer on March 16, 1998, 11:21 GMT. The visible modulates the red, 3.7-μm reflectance (greater for clouds composed of smaller particles) for the green and temperature for the blue. Therefore, more red clouds contain larger particles, whereas more yellow clouds contain smaller particles. The blue background is the surface. Dust is evident by the obscuration of the sea surface in frames 1 and 4. Heavy blur due to dust is observed in frames 5 and 6. Analyses of clouds in the frames are given in Fig. 2.

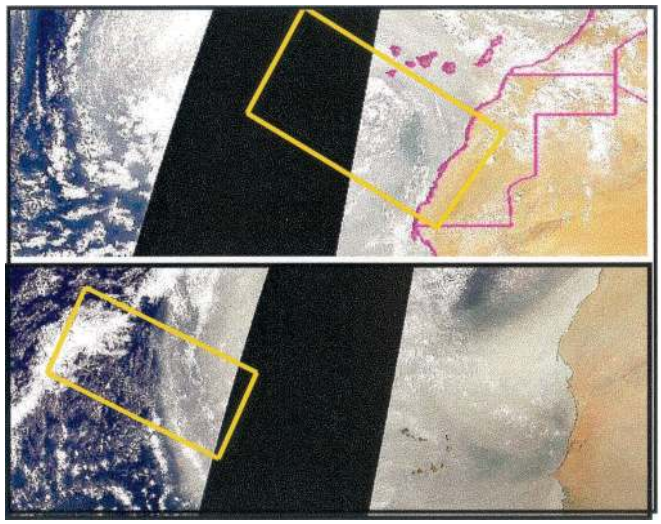

Fig. 3. Dust blowing off the Western Sahara interacts with the marine clouds over the Eastern Atlantic. These Seawifs satellite images are for the 1st (*Upper*) and 5th (*Lower*) of March 2000 (12 GMT). The rectangles mark the areas covered by TRMM overpasses for the two cases.

south west of Cyprus was 5%. Given these observations, and with cloud tops extending above the top of the dust layer, and given the fact that contribution of the 3.7-μm reflectance comes only from the top 100–200 m of the cloud, the direct contribution of the dust reflectance to the cloud reflectance and induced errors to the retrieved effective radius can be neglected.

Recently, radar measurements from the Tropical Rainfall Measuring Mission (TRMM) satellite have been used to substantiate the microphysical cloud inferences of suppression of coalescence and precipitation inferred from the classification of Rosenfeld and Lensky (5) for smoke-laden (8) and polluted clouds (2). Unfortunately, TRMM radar measurements are not available for the clouds formed in the 1998 dust storm over the Eastern Mediterranean. Therefore, cloud microphysics and rain formation in clouds that formed in heavy dust storms were studied by using TRMM off the Western Sahara over the Atlantic Ocean. According to Fig. 3, the visible wakes in the dust layer downwind of the islands and the overlap between the cloud organization and dust features indicate that the clouds developed within the dust-laden air. According to Fig. 4, the aerosols in the TRMM-analyzed regions shown in Fig. 5, are desert dust, with no contribution of biomass burning or sulfur aerosols.

The T-r_e relations in the clouds shown in Fig. 5 demonstrate that thick marine stratocumulus clouds growing in regions with heavy desert dust (line 5 of Fig. 6) have r_e well below the 14-μm precipitation threshold. The r_e increases with the distance into the sea and with decreasing amount of dust, eventually producing precipitation that is observed by the precipitation radar onboard the TRMM satellite, which can detect a minimum

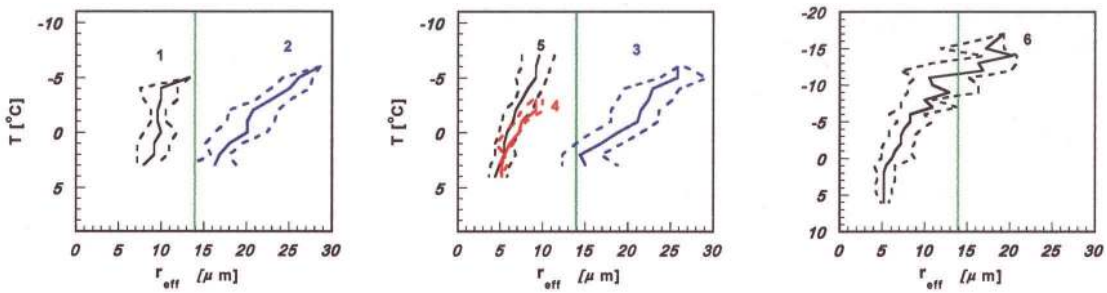

Fig. 2. Analysis of the T-r_e relations for the clouds in Fig. 1. T is the temperature, and r_e is the cloud particle effective radius for the clouds in the six frames in Fig. 1, respectively. Plotted are the 15% (long dashed line) 50% (solid line), and 85% (short dashed line) percentiles of the r_e for each 1°C interval. The black and red lines correspond to the dusty boxes. The vertical green line marks the 14-μm precipitation threshold. A full description of the meaning of the T-r_e charts is given in ref. 5.

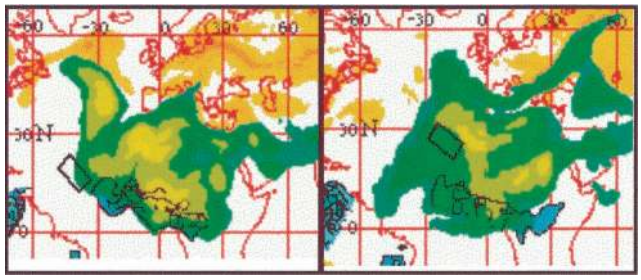

Fig. 4. An aerosol map for the 1st (*Left*) and 5th (*Right*) of March 2000 (12 GMT), obtained from the Glabat Aerosol data. The optical depth is shown in blue for smoke, green for desert dust, and orange for sulfates. The black contours extending from central Africa to the south part of West Africa enclose areas of mixed smoke with dust. The TRMM coverage is shown as the small frames to the west of the Sahara, residing clearly in the dust-only areas. The map was produced by the Navy Aerosol Analysis and Prediction System (http://www.nrlmry.navy.mil/aerosol/Docs/nrlmryonrprop.html).

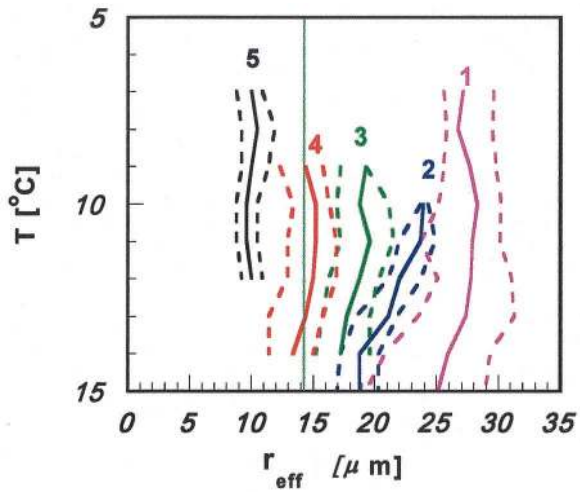

Fig. 6. Analysis of the T-r_e relations for marine stratocumulus forming with different amounts of desert dust. Lines 1–4 correspond to frames 1–4 in Fig. 5, which go from dust free (frames 1 and 2) to dust-laden air (frame 4). Line 5 corresponds to clouds forming in heavy dust storm, as shown in Fig. 4 *Right*. Note the decreasing r_e with increasing amounts of dust from lines 1 to 5.

precipitation intensity of 0.7 mm/hr. The slight precipitation can be seen in frames 1 and 2 of Fig. 5 as white squares. For a given cloud depth, the increase of r_e leads to the onset of precipitation (see lines 2–5 in Fig. 6). The dust-induced reduced r_e and suppressed precipitation are further supported by the observation of comparable amounts of cloud water within these clouds, indicated by similar maximum values of the vertically polarized 85-GHz brightness temperatures by the TRMM passive microwave imager. The progressive enhancement of the coalescence farther away from the dust source can be attributed to the decreasing amounts of dust, probably aided by the wet coagulation and cleaning process described by Wurzler *et al.* (9).

Aircraft Observations of Cloud-Dust Interactions

Simultaneous to the satellite observations, two flights of an aircraft equipped for cloud physics measurements were undertaken in the March 1998 storm over Israel. The aircraft was equipped with a 2DC optical array for visualization of particles up to a size of 0.8 mm, a King hot wire instrument for measuring cloud liquid water contents, a thermometer, and a global positioning system navigation system. The first flight was in the dust-free air [east of frame 3 in Fig. 1, March 16, 1998 13:28–14:43 Greenwich mean time (GMT)]. The clouds contained large amounts of drizzle and warm rain, which froze at about −7°C and formed high concentrations of frozen drops and graupel. Maximum liquid water content reached 3 g·m^{-3} at the −8.5°C isotherm level, which was near the measured cloud tops. The aircraft measurements validate the satellite inference of active coalescence and warm rain outside the dusty areas (line 3 of Fig. 2).

During the second flight (March 17, 1998, 11:12–15:31 GMT) the dust was so heavy that the ground was not seen from a height of 3 km, and yellow ice rimed on the airplane. In contrast to the clouds that formed in the clean air, only a few drizzle particles were observed, mainly over the sea. Over land, isolated frozen drops and graupel were formed in clouds near the −8°C isotherm, and the maximum liquid water contents reached 3

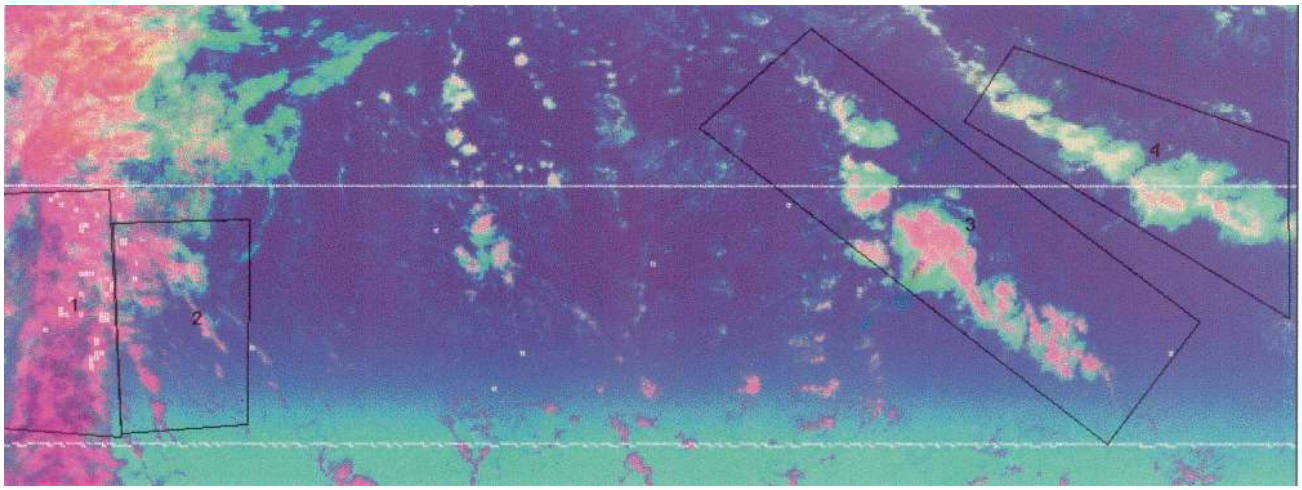

Fig. 5. Satellite visualization showing the impact of Saharan dust on cloud microstructure and precipitation. The image was taken by the TRMM visible and IR detector on March 1, 2000 16:06 GMT, west of the Sahara (36W-46W). The visible modulates the red, 3.7-μm reflectance for green, and T for the blue. The white patches in frames 1 and 2 represent precipitation echoes observed by the TRMM precipitation radar. The two parallel lines delimit the 220-km precipitation radar swath, oriented from the dust-free zone in the northwest to the dusty area in the southeast (left to right, respectively), as shown in Fig. 4. The image shows clouds with large droplets (red colors) and precipitation in the dust-free area (1 and 2), gradually reducing the size of droplets and decreasing the precipitation in transition to the dusty area (frames 3 and 4).

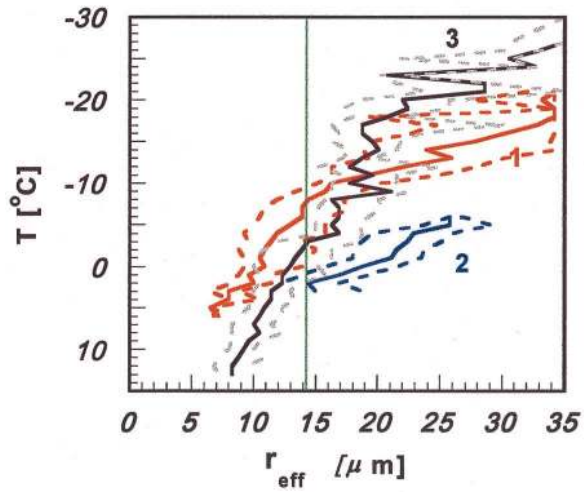

Fig. 7. Analysis of the satellite retrieved T-r_e relations for the clouds in the region sampled by the aircraft. Line 1 (red) pertains to the dust-laden clouds on March 17, 1998; line 2 (blue) pertains to the dust-free clouds on March 16, 1998. For comparison, clouds formed in smoke are presented in line 3 (black), as measured and validated by aircraft on May 2, 1998 in Thailand (11).

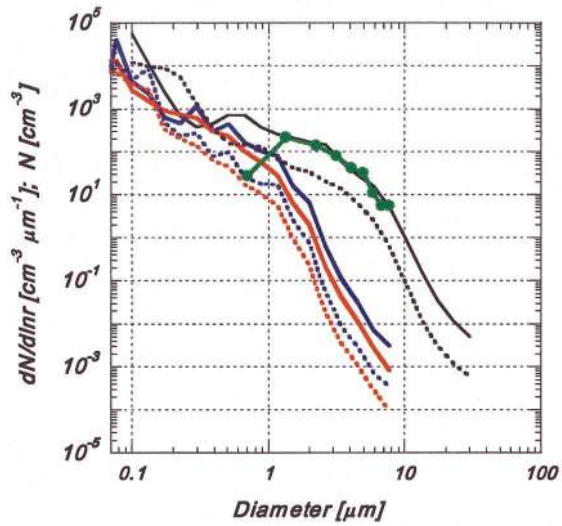

Fig. 8. The particle size distribution during Saharan dust storms. The green points are *in situ* measurements of dust concentrations made at Tel Aviv during the storm of March 17, 1998. The black lines represent concentrations retrieved from sky radiometers in Sde-Boker (solid line) and Cape Verde (dashed line) during Saharan dust storms. The CCN concentrations are calculated by assuming that all of the vertically integrated particles are concentrated in a 1-km vertical column. The conversion of dust into CCN concentrations is represented by the blue lines (Sde-Boker, solid; Cape Verde, dashed). The red lines (Sde-Boker, solid; Cape Verde, dashed) represent the cumulative concentrations of the CCN, beginning with the largest bin size.

g·m^{-3}, similar to that measured in the dust-free clouds. A large number of mostly dendritic ice crystals appeared at -12°C to -18°C with only slow growth with height. The slow growth of the ice particles left most of the cloud water in the growing convective elements unfrozen, reaching a maximum of 3.5 g·m^{-3} at -18°C and 2.6 g·m^{-3} at -21.5°C. The clouds totally glaciated rapidly at colder temperatures. Obviously, coalescence was not very active in these clouds, indicating a lack of a large number of giant CCN. Desert dust advected to Israel is known to be active as ice nuclei at $T < -11$°C (10). The dust probably nucleated the ice crystals, which grew slowly because of the small size of the cloud droplets and the weak coalescence.

The aircraft and satellite measurements provide a consistent picture. The satellite retrievals (see Fig. 7, line 1) show that the median r_e remained below the precipitation threshold of 14 μm until $T = -8$°C, where the first graupel were observed by the aircraft. The aircraft observation of progressive development of the ice phase at -11°C $< T < -22$°C corroborates the satellite-retrieved steep increase of r_e at $T < -10$°C. The aircraft measurements show that precipitation processes are much less developed in the dust-laden clouds compared with the dust-free clouds.

These observations suggest that desert dust inhibit the precipitation-forming processes mainly by suppression of droplet coalescence. Comparison to clouds formed in smoke (see one example in Fig. 7, trace 3) shows typically slower growth of cloud particles and precipitation with height in the smoky clouds compared with the dusty clouds. The clouds in the smoky air, shown in Fig. 7, had supercooled water extending to much lower T than the clouds in the dusty air, despite their warmer base. Aircraft measurements showed that these smoke-laden clouds had supercooled water of 2.5 g·m^{-3} at -32°C (11). The differences between clouds ingesting dust and smoke particles are greatest at the supercooled levels. Therefore, desert dust appears to inhibit precipitation less strongly than smoke.

CCN Activity of the Desert Dust

Mineral dust particles affect the clouds through their activity as CCN and ice nuclei. The CCN activity of aerosols is strongly related to their content of water-soluble material. The CCN content of the dust was characterized by chemical analysis of individual particles collected near the ground during the storm peak (10:00 GMT, March 16, 1998) (12). The morphology of individual particles was studied by using a scanning electron microscope (SEM) equipped with an energy dispersive system, and the elemental composition was determined quantitatively by using established methods (3, 13). It was found that 65% of the particles contained sulfur, which on the average lies on the surface of the particles (12). The sulfur mass (in g) in a particle of diameter d is given by

$$\mathrm{Log}(S) = 2.13\ \mathrm{Log}(d) - 13.44. \qquad [1]$$

It appears that the sulfur coating did not result from reactions or deposition that occurred in the atmosphere, but rather from soil-related processes that occurred in the source region. Only 15% of the sulfur-containing particles were clearly gypsum (Ca/S≈1). However, many pure calcite particles were present in the sample. Several studies have shown that gypsum ($CaSO_4 \cdot 2H_2O$) is often a product of a chemical reaction of atmospheric SO_2 on the surface of calcite aerosols ($CaCO_3$) (14–18). The presence of pure calcite particles suggest that the sulfur in the sample did not result from reactions or deposition that occurred in the atmosphere, or from chemical transformation on the sampling filters due to high SO_2 levels, but must have its origin in the source region. Sulfur also can accumulate on the particles by other atmospheric processes such as S(IV) oxidation in the droplets, scavenging of H_2SO_4, and in-cloud processing. In such cases, sulfuric acid is clearly identified by a SEM equipped with an energy dispersive system as condensed sphere-like sulfur particles (3, 19–21). No sulfuric acid aerosols or other particles that show only sulfur (such as ammonium sulfate or ammonium bisulfate) were observed in the SEM equipped with an energy dispersive system spectra. Sulfur, which can possibly arise from tiny aerosols not observed in SEM, was not detected on the filter. In addition, H_2SO_4 and NaCl particles, the common tracers of air masses that passed over the Mediterranean Sea, were not detected in the present sample. Finally, 5-days-back trajectory

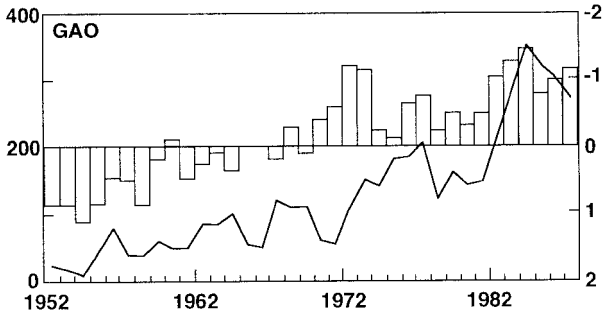

Fig. 9. Frequency of dust occurrence from 1957 to 1987 at Gao, 16°16′N, 00°02′W, (solid line, left vertical axis) compared with rainfall anomalies (bar graph, right vertical axis) for the Sahelian region as a whole. Rainfall is expressed as a regionally averaged, standardized departure (departure from the long-term mean divided by the standard departure), but the axis of the rainfall graph is inverted to facilitate comparison with dust occurrence. Dust is represented by the number of days with dust haze. [Reproduced with permission from ref. 32 (Copyright 1997, American Meterological Society)].

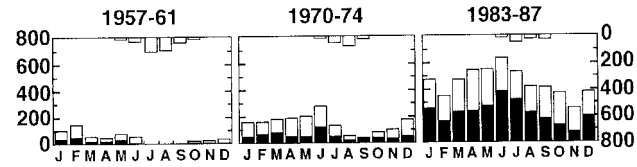

Fig. 10. Mean monthly rainfall and number of hours with visibility reduced to less than 5 km (filled bars) and less than 10 km (empty bars) at Gao during three periods: 1957–1961, 1970–1974, and 1983–1987. The number of hours per month of reduced visibility is on the left-hand vertical axis. The monthly rainfall is shown at the top of each diagram, with the amount in mm indicated on the right-hand vertical axis. [Reproduced with permission from ref. 32 (Copyright 1997, American Meterological Society)].

calculations show that indeed the storm did not pass over the Mediterranean and encountered mainly unpopulated and pristine areas (12). Therefore, we conclude that the desert dust was the only significant source for the CCN in this case study, so that the observed differences in the clouds microstructure can be uniquely related to the CCN activity of the dust.

The particles in each SEM image were counted and scaled to the full filter size. Using the known pumping flow rate and the sampling time, an average number of 550 particles cm^{-3} was determined. The size distribution of the collected particles in the range between 0.5 and 10 μm also was obtained. Although this distribution is truncated at 0.5 μm, it is compared with the complete aerosol size distribution obtained by monitoring the absorption and scattering of solar radiation using sun photometers [part of the Aerosol Robotic Network (AERONET) (22)] situated in Sde-Boker (Israel) during another heavy dust storm (April 19, 2000). The distributions were retrieved by using the method of Dubovik *et al.*(23, 24), assuming a depth of the dust layer of 1 km. The two distributions are in excellent agreement as can be seen in Fig. 8, except for the measurement at the 0.5-μm size, for which the SEM method may underestimate the number of particles due to the difficulties in measuring such small particles in the SEM images.

The CCN activity of mineral dust particles was calculated based on their size and soluble content. The dust particles were converted to equivalent CCN particles composed of NaCl and having the same activity. We divided the treatment to particles that contain soluble material and those that do not.

Particles that contain soluble material were normalized to NaCl particles having the same number of ions.

Insoluble particles are assumed to become readily wet in water super saturation. They therefore can be treated effectively as pure water drops having the same size as the wet dust particles. To account for the creation of these drops we must express the insoluble part as a soluble CCN that initially grows to the size of these wet insoluble particles. This is done by assigning a NaCl particle that is 1/5 of the size of the wet dust particle. This treatment follows Ivanova *et al*. (25), who showed that a droplet formed on a CCN behaves practically as a pure water drop after it expands to a size five times larger than the original NaCl dry particle.

The equivalent of NaCl CCN in the dust was calculated by using the size distribution and the determined sulfur mass. It is implicitly assumed here that Eq. **1** holds for all sizes. The soluble material is assumed to be the sulfur and its mass was calculated for each particle size by using Eq. **1**. It is assumed that for each mol of sulfur there are 2 mol of counter ions. The fraction of insoluble particles in the March 1998 dust storm was 35%. The results of such transformations for the March 1998 dust storm and the AERONET measurements of typical dust storms over Sde-Boker (Israel) and Cape Verde (West Africa) are shown in Fig. 8. The AERONET data for Cape Verde are the average of all of the 1995–1999 measurements during dust situations with an optical depth of 0.7 at wavelength of 0.44 μm. Assuming a depth of 1 km for the dust layer, the concentrations of CCN $>$ 0.067 μm are 13,550 cm^{-3} and 7,100 cm^{-3} in Sde-Boker and Cape Verde, respectively. The concentrations of the large CCN ($d >$ 2 μm) at the two sites are 2 and 0.2 cm^{-3}, respectively. The transformation shown in Fig. 8 shifts the dust particle distribution to much smaller sizes of CCN, leading to the observed Twomey effect and the reduced droplet coalescence.

Climatic Perspective of Dust-Cloud Interactions

In this study we show the effect of mineral dust on cloud microphysics. Based on the observations the following picture emerges: Saharan desert dust provides very large concentrations of CCN, mostly in the small size range. These lead to formation of clouds that are dominated by small droplets, leading to little coalescence and suppressed precipitation. This is similar to the observed effect of smoke and air pollution on clouds (2, 8). Due to the large spatial and temporal extent of desert dust in the atmosphere (26), the interactions of desert dust with clouds can have substantial climatic impacts. The decrease in r_e increases the albedo of the clouds in the same manner that smoke and air pollution do (1), partially counteracting the warming due to the increased greenhouse gases (27). As important as the radiative effect is the impact of the dust on precipitation. It has been commonly believed that the larger concentrations of large and giant CCN, regardless of the distribution of the smaller CCN, can lead to enhanced coalescence and precipitation in convective clouds (4). However, here we show that the coalescence-suppressing effects of the large concentrations of small dust particles and the insoluble larger particles dominate over the enhancing effects of the giant CCN. In addition, the desert dust has greater ice nucleating activity compared with smoke. The existence of giant CCN and the ice nucleating activity of the dust probably explain the larger increase of the r_e with height in dusty clouds compared with clouds affected by smoke from biomass burning or from air pollution.

Kaufman and Fraser (28) have measured an average of r_e = 15 μm for clouds with $T > 270$ K over the Amazon basin, when not affected by smoke, which means that these clouds form in clean air with a relatively small concentration of CCN. A recent satellite study (29) shows that tropical clouds over Africa have considerably smaller r_e than over the Amazon. Those authors suggest that this difference might be caused by the higher concentrations of aerosols over Africa due to the proximity of deserts. They also suspected that the difference in r_e might lead

to a reduction in the precipitation efficiency of the African clouds by up to a factor of 2, compared with the clouds over the Amazon. It is important to note that the detrimental impact on precipitation shown here occurs on the background of relatively clean maritime and continental-tropical air, whereas the previous indications for desert dust enhancing coalescence (3, 4) occur on the background of desert dust interacting with already polluted air by sulfur emissions, which were already shown to strongly suppress precipitation (2).

It should be noted that short-lived convective clouds are the most sensitive to the impact of aerosols on precipitation, because the rate of cloud water conversion into precipitation has to compete with the rate of cloud water loss due to mixing and evaporation with the ambient air. Large-scale synoptically forced cloud systems are typically longer lived, and thus less vulnerable to the detrimental impact of smoke and dust on the precipitation.

In addition to the detrimental microphysical impact of dust on already formed convective clouds, dust can affect precipitation formation through radiative interactions. For example, stabilization of the daytime boundary layer due to absorption solar radiation and local warming can suppress the very formation of the convective clouds (30). The warming of the lower half of the troposphere due to absorption by dust was shown to be an important climatic factor in the Sahel (31).

In this study we suggest that the desert dust might contribute significantly to the observed reduction of r_e and precipitation over Africa. The observed correlation between the trends of declining precipitation and increasing dust during the rainy season in the Sahel [see Figs. 9 and 10, excerpted from Mbourou *et al.* (32)] can now be subject to another interpretation. The higher dust frequency is not necessarily a result of the decreased rainfall, but rather its cause. Anthropogenic activities, such as grazing and cultivation, expose and disrupt the topsoil, thus enhancing dust emissions from the surface (33). The dust therefore could provide a mechanism for initiating a desertification feedback cycle. Such a process may have contributed to the desertification of the Sahel during recent decades (34). Further research should be undertaken to develop a more complete understanding of these interactions.

Discussions with A. Falkovich, S. Wurzler, W. L. Woodley, and S. Berkowich are acknowledged. We thank Brent Holben, Oleg Dubovik, and Alexander Smirnov of the National Aeronautics and Space Administration/Goddard Space Flight Center for providing and assisting in the interpretation of the AERONET data. Y.R. is the incumbent of the William Z. and Eda Bess Novick career development chair. This study was funded by the Israeli Space Agency, the Israeli Water Commission, and the German-Israeli Science Foundation.

1. Twomey, S., Gall, R. & Leuthold, M. (1987) *Boundary Layer Metorol.* **41,** 335–348.
2. Rosenfeld, D. (2000) *Science* **287,** 1793–1796.
3. Levin, Z., Ganor, E. & Gladstein, V. (1996) *J. Appl. Meteorol.* **35,** 1511–1523.
4. Yin, Y., Levin, Z., Reisin, T. G. & Tzivion, S. (2000) *Atmos. Res.* **53,** 91–116.
5. Rosenfeld, D. & Lensky, I. M. (1998) *Bull. Am. Meteorol. Soc.* **79,** 2457–2476.
6. Rosenfeld, D. & Gutman, G. (1994) *Atmos. Res.* **34,** 259–283.
7. Levi, Y. (1997) Ph.D thesis (The Hebrew University, Jerusalem, Israel).
8. Rosenfeld, D. (1999) *Geophys. Res. Lett.* **26,** 3105–3108.
9. Wurzler, S., Reisin, T. G. & Levin, Z. (2000) *J. Geophys. Res.* **105,** 4501–4512.
10. Levi, Y. & Rosenfeld, D. (1996) *J. Appl. Meteorol.* **35,** 1494–1501.
11. Rosenfeld, D. & Woodley, W. L. (1999) *Proceedings of the Seventh World Meterological Organization (WMO)* (Chiang Mai, Thailand), pp. 17–20.
12. Falkovich, A., Ganor, E., Levin, Z., Formenti, P. & Rudich, Y. (2001) *J. Geophys. Res.*, in press.
13. Pardess, D., Levin, Z. & Ganor, E. (1992) *Atmos. Environ.* **26,** 675–680.
14. Andreae, M. O., Charlson, R. J., Bruynseels, F., Storms, H., Van Grieken, R. & Maenhaut, W. (1986) *Science* **232,** 1620–1623.
15. Carmichael, G. R., Zhang, Y., Chen, L. L., Hong, M. S. & Ueda, H. (1996) *Atmos. Environ.* **30,** 2407–2416.
16. Dentener, F. J., Carmichael, G. R., Zhang, Y., Lelieveld, J. & Crutzen, P. J. (1996) *J. Geophys. Res.* **101,** 22869–22889.
17. Mamane, Y. & Gottlieb, J. (1989) *J. Aerosol Sci.* **20,** 303–311.
18. Okada, K., Kobayashi, A., Iwasaka, Y., Naruse, H., Tanaka, T. & Nemoto, O. (1987) *Met. Soc. Japan* **67,** 515–521.
19. Ganor, E. (1999) *Atmos. Environ.* **33,** 4235–4242.
20. Ganor, E., Levin, Z. & Pardess, D. (1993) *Atmos. Environ.* **27,** 1821–1832.
21. Ganor, E., Levin, Z. & Van Grieken, R. (1998) *Atmos. Environ.* **32,** 1631–1642.
22. Holben, B. N., Eck, T. F., Slutsker, I., Tanre, D., Buis, J. P., Setzer, A., Vermote, E., Reagan, J. A., Kaufman, Y. J., Nakajima, T., *et al*. (1998) *Remote Sens. Environ.* **66,** 1–16.
23. Dubovik, O., Smirnov, A., Holben, B. N., King, M. D., Kaufman, Y. J., Eck, T. F. & Slutsker, I. (2000) *J. Geophys. Res.* **105,** 9791–9806.
24. Dubovik, O. & King, M. D. (2000) *J. Geophy. Res.* **105,** 20673–20696.
25. Ivanova, E. T., Kogan, Y. L., Mazin, I. P. & Permgakov, M. S. (1977) *Izv. Atmos. Phys.* **13,** 1193–1201.
26. Prospero, J. M. (1999) *Proc. Natl. Acad. Sci. USA* **96,** 3396–3403.
27. Houghton, J. T., Meira Filho, L. G., Callender, B. A., Harris, N., Kattenberg, A. & Maskell, K., eds. (1996) *Climate Change 1995: The Science of Climate Change, Contribution of Working Group I to the Second Assessment Report of the Intergovernmental Panel on Climate Change (IPCC)* (Cambridge Univ. Press, Cambridge, U.K.).
28. Kaufman, Y. J. & Fraser, R. S. (1997) *Science* **277,** 1636–1639.
29. McCollum, J. R., Gruber, A. & Ba, M. B. (2000) *J. Appl. Meteorol.* **39,** 666–679.
30. Druhet, A. & Durand, P. (1984) *Boundary Layer Meteorol.* **28,** 51–77.
31. Alpert, P., Kaufman, Y. J., Shay-El, Y., Tanre, D., da Silva, A., Schubert, S. & Joseph, J. H. (1998) *Nature (London)* **395,** 367–370.
32. Mbourou, G. N., Bertrand, J. J. & Nicholson, S. E. (1997) *J. Appl. Meteorol.* **36,** 868–882.
33. Tegen, I. & Fung, I. (1995) *J. Geophys. Res.* **100,** 18707–18726.
34. Nicholson, S. (2000) *Rev. Geophys.* **38,** 117–139.